Supporting Information

Bicontinuous Transition Metal Phosphides/rGO Binder-free Electrodes: Generalized Synthesis and Excellent Cycling Stability for Sodium Storage

*Yanpeng Fu,[1,#] Zhibo Zhang,[2, #] Changbao Zhu,[2,]**

Experimental Section

Preparation of multiple metal phosphides @rGO composites:

In a typical procedure, the metal ion sources ($CuSO_4 \cdot 5H_2O$, $C_{15}H_{21}FeO_6$, $Co(NO_3)_2$), $NH_4H_2PO_4$, citric acid with a molar ratio of 3:2:1 were dissolved in 0.5 ml water to form a transparent solution. Then 1 ml GO (2 mg mL^{-1}; sheet size < 500 nm; purchased form XFNANO company) were added to the above transparent solution, followed by the addition of 1,2-propanol. Then the precursor solution was extracted into a syringe with a nozzle diameter of 1.2 mm. The distance between the nozzle and the substrate was kept at 2.5 cm. The flow rate of well dispersed solution maintained at 10 μL min^{-1}. Copper foil was selected as a substrate and a current collector, which was preheated to 190 ºC. During the ESD process, a high voltage of 7.5 kV was applied. The as-deposited samples were then annealed at 700ºC for 10min with a heating rate of 10 °C min^{-1} under Ar/H_2 atmosphere in a tube furnace.

Material Characterization:

XRD measurements were carried out with a Rigaku D/max 2200 VPC X-ray

diffractometer. SEM images and EDS spectrometry were measured using a Gemini SEM 500. TEM and HRTEM tests were performed using the FEI Tecnai G2 F30. Raman spectrum was recorded using FEX (NOST Korea) with a 532 nm diode laser. The carbon content was measured by a CHNS elemental analyzer.

Electrochemical Characterization:

The 3D porous Cu_3P/rGO nanocomposite deposited on Cu foils was used as working electrode directly without any binder and conductivity additives. Sodium metal and glass fiber was used as counter electrode and separator, respectively. The electrolyte was 1 M solution of $NaClO_4$ in the propylene carbonate (PC) with 5% fluoroethylene carbonate (FEC). The sodium-ion half cells were assembled as CR2032 coin cells in a glove box under Ar atmosphere (O_2<0.1 ppm, H_2O<0.1 ppm). The galvanostatic charge/discharge measurements were carried out on Neware BTS-4000 battery test system at a voltage from 0.01-2.8 V. The CV curves were acquired from CHI 660E electrochemical workstation.

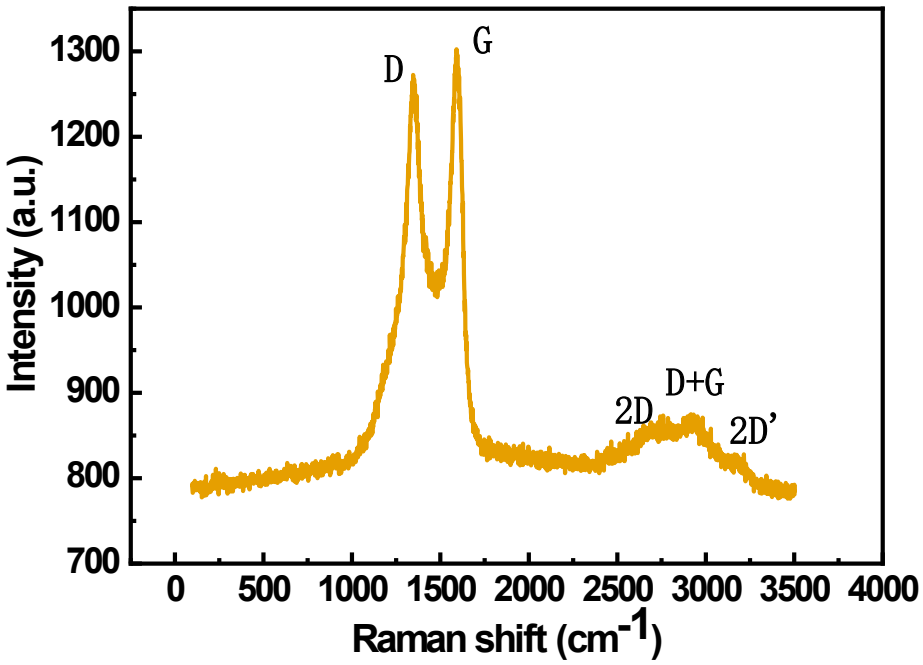

Figure S1: Raman spectrum of the Cu_3P/rGO nanocomposite.

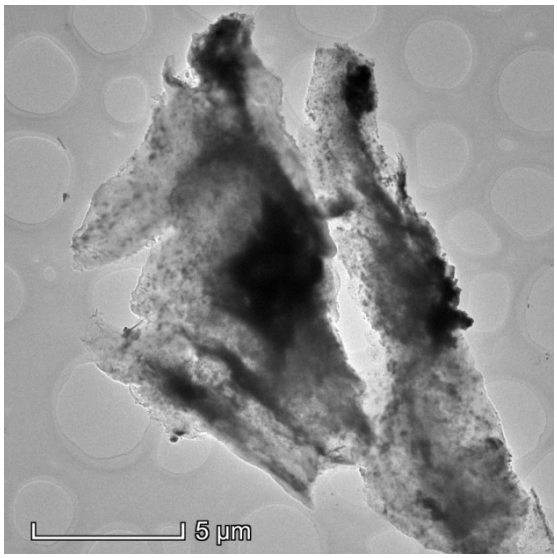

Figure S2: TEM images of the as prepared 3D porous Cu_3P/rGO nanocomposite.

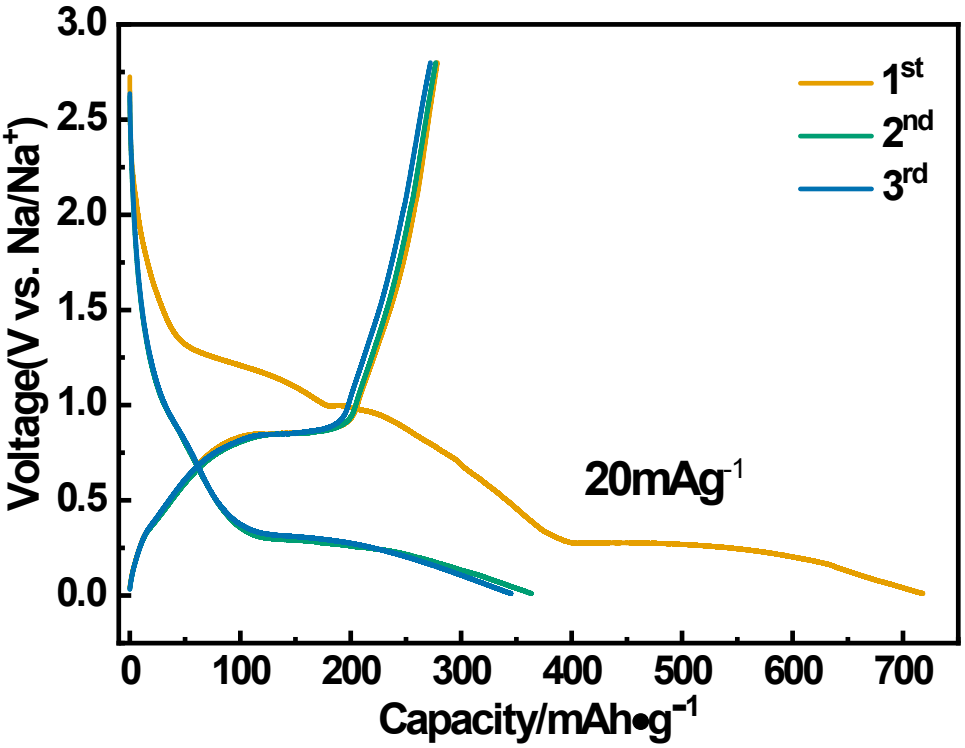

Figure S3: The galvanostatic charge and discharge profiles of the 3D porous Cu_3P/rGO nanocomposite at a current density of 20 mA g^{-1} in the first three cycles.

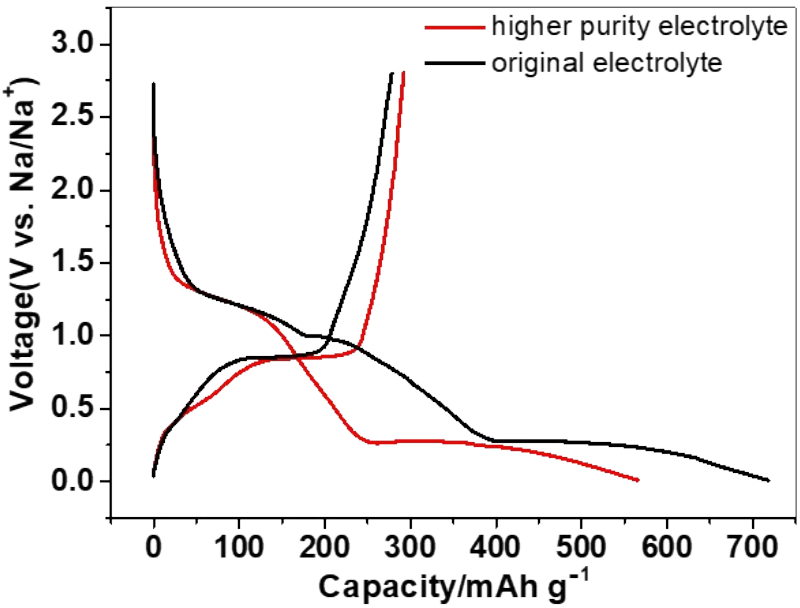

Figure S4. The galvanostatic charge and discharge profiles of the 3D porous Cu_3P/rGO nanocomposite at a current density of 20 mA g^{-1} for the first charge-discharge cycle using the electrolytes with different purities, which demonstrates the initial coulomb efficiency can be improved by electrolyte optimization.

Table S1: Comparison of cycling performance of metal-rich phosphides as SIB anodes

Materials	Synthetic method	Cycling performance			Theoretical capacity (mAh g^{-1})	Ref.
		Current density (mA g^{-1})	Cycle number	Capacity (mAh g^{-1})		
3D porous Cu_3P	Electrospray deposition	1000	2500	118	363	This work
Cu_3P NWs	Aqueous reaction /phosphorization	1000	260	133.8	363	S1
Cu_3P/C	Solution phase/annealing	100	100	221	363	S2
Co_2P-3D PNC	Blowing method /phosphidation	500	700	271	540	S3
Sn_4P_3@C	Hydrothermal/phosphorization	1000	400	360	1132	S4
Sn_4P_3@C sphere	Aerosol spray-pyrolysis	100	120	700	1132	S5
Yolk-shell Ni_2P	Hydrothermal/phosphidation	200	100	181	542	S6
Ni_2P/graphene/ Ni_2P	Hydrothermal/phosphidation	500	300	188	542	S7
MoP nanorod/C	Solid phase reaction	100	800	398	633	S8
FeP nano array	Hydrothermal/phosphidation	200	100	548	924	S9

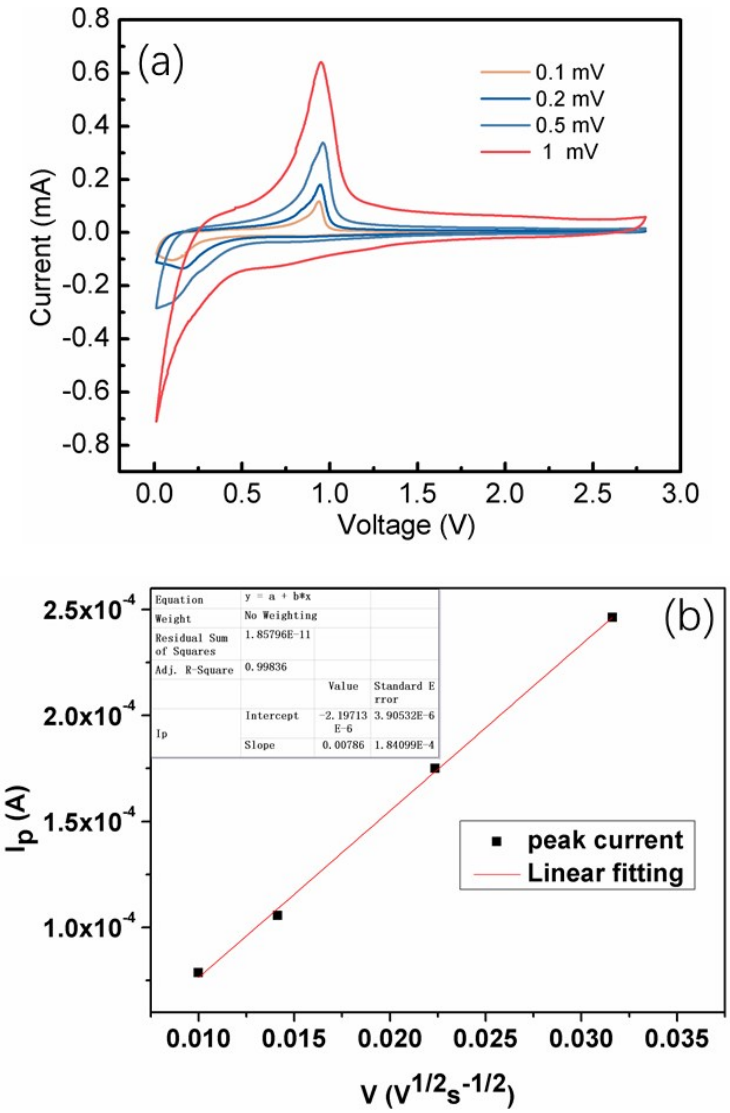

Figure S5: a) CV curves of the 3D porous Cu_3P@C electrodes at different scan rates from 0.1 mV s^{-1} to 1 mV s^{-1}; b) Peak current I_p as a function of square root of scan rate.

The energy storage process is divided into two categories: the diffusion and capacitive controlled process. To further investigate the superior Na-ion storage performance of the 3D porous Cu_3P@C electrodes, CV tests at various scan rates from 0.1 to 1 mV s^{-1} were carried out to decide the controlled process either by diffusion or

capacitive. Generally, the measured current (i) and the corresponding sweep rate (v) obey the following relationship [S10]

$$i=av^b$$

where a and b are empirical parameters. The b value of 0.5 represents the diffusion controlled electrochemical reaction, while b value of 1 indicates a capacitive controlled process. In this Cu_3P@C electrodes, the b values for anodic peaks obtained by plotting log(i) versus log(v) is 0.503, which suggests that the electrochemical process is controlled by the diffusion behavior.

The determination of the effective diffusion coefficient can be calculated by applying Randles–Sevcik analysis on CV measurements at different scan rates.[S10] Using the geometric electrode area an apparent diffusion coefficient of 2.52×10^{-19} cm^2/s is obtained for 3D porous Cu_3P@C electrodes. This value is in accordance with the previous report.[S2]

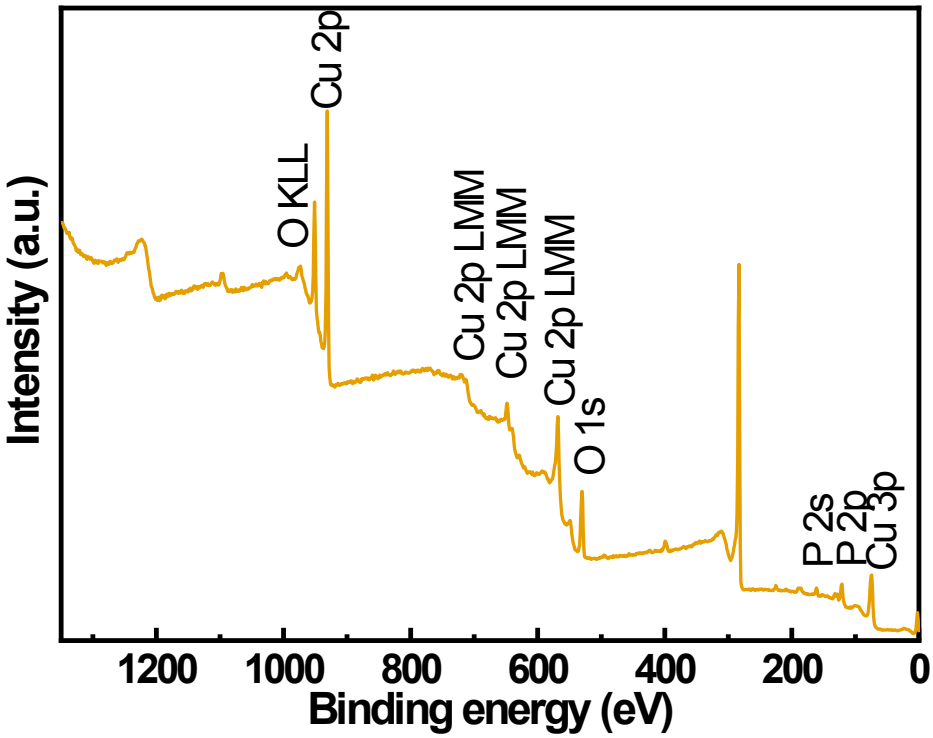

Figure S6: XPS survey of the as synthesized Cu_3P/rGO nanocomposite.

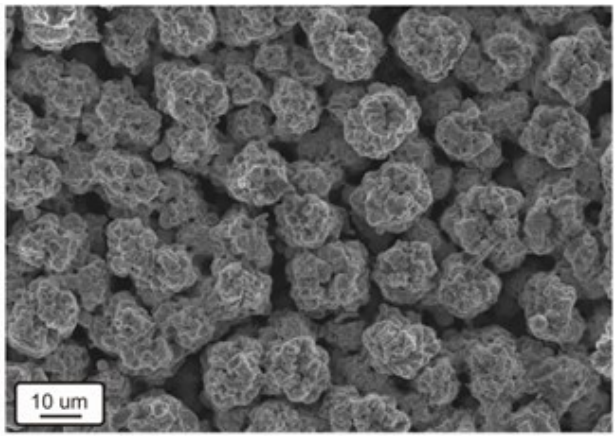

Figure S7: SEM image of the 3D porous Cu_3P/rGO electrodes after 800 cycles at a current density of 100 mA g^{-1}.

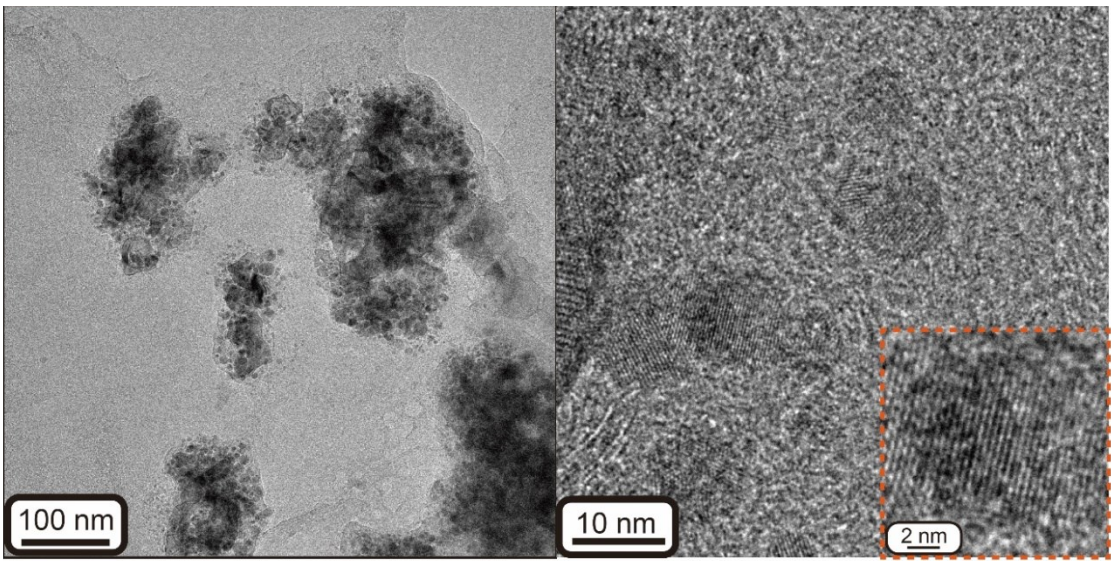

Figure S8 a-b): TEM and HRTEM images of the Cu_3P/rGO nanocomposite after 800 cycles at a current density of 100 mA g^{-1}.

Reference :

S1. M. P. Fan, Y. Chen, Y. H. Xie, T. Z. Yang, X. W. Shen, N. Xu, H. Y. Yu and C. L. Yan, *Adv Funct Mater*, 2016, **26**, 5019-5027.
S2. M. H. Kong, H. H. Song and J. S. Zhou, *Adv Energy Mater*, 2018, **8**.
S3. D. Zhou and L. Z. Fan, *J Mater Chem A*, 2018, **6**, 2139-2147.
S4. J. Liu, P. Kopold, C. Wu, P. A. van Aken, J. Maier and Y. Yu, *Energ Environ Sci*, 2015, **8**, 3531-3538.
S5. X. L. Fan, T. Gao, C. Luo, F. Wang, J. K. Hu and C. S. Wang, *Nano Energy*, 2017, **38**, 350-357.
S6. C. Wu, P. Kopoid, P. A. van Aken, J. Maier and Y. Yu, *Adv Mater*, 2017, **29**.
S7. C. F. Dong, L. J. Guo, Y. Y. He, C. J. Chen, Y. T. Qian, Y. N. Chen and L. Q. Xu, *Energy Storage Mater*, 2018, **15**, 234-241.
S8. Z. D. Huang, H. S. Hou, C. Wang, S. M. Li, Y. Zhang and X. B. Ji, *Chem Mater*, 2017, **29**, 7313-7322.
S9. Y. Wang, C. J. Wu, Z. G. Wu, G. W. Cui, F. Y. Xie, X. D. Guo and X. P. Sun, *Chem Commun*, 2018, **54**, 9341-9344.
S10. H. Lindström, S. Södergren, A. Solbrand, H. Rensmo, J. Hjelm, A. Hagfeldt and S. E. Lindquist, *Journal of Physical Chemistry B*, 1997, **101**, 7717–7722.